BRAIN CONNECTIVITY
Volume 2, Number 6, 2012

DOI: 10.1089/brain.2012.0105-Rev

Disrupted Brain Networks in the Aging HIV+ Population

Neda Jahanshad,[1,2,*] Victor G. Valcour,[3,4,*] Talia M. Nir,[1] Omid Kohannim,[1] Edgar Busovaca,[3] Krista Nicolas,[3] and Paul M. Thompson[1]

Abstract

Antiretroviral therapies have become widely available, and as a result, individuals infected with the human immunodeficiency virus (HIV) are living longer, and becoming integrated into the geriatric population. Around half of the HIV+ population shows some degree of cognitive impairment, but it is unknown how their neural networks and brain connectivity compare to those of noninfected people. Here we combined magnetic resonance imaging-based cortical parcellations with high angular resolution diffusion tensor imaging tractography in 55 HIV-seropositive patients and 30 age-matched controls, to map white matter connections between cortical regions. We set out to determine selective virus-associated disruptions in the brain's structural network. All individuals in this study were aged 60–80, with full access to antiretroviral therapy. Frontal and motor connections were compromised in HIV+ individuals. HIV+ people who carried the apolipoprotein E4 allele (ApoE4) genotype—which puts them at even greater risk for neurodegeneration—showed additional network structure deficits in temporal and parietal connections. The ApoE4 genotype interacted with duration of illness. Carriers showed greater brain network inefficiencies the longer they were infected. Neural network deficiencies in HIV+ populations exceed those typical of normal aging, and are worse in those genetically predisposed to brain degeneration. This work isolates neuropathological alterations in HIV+ elders, even when treated with antiretroviral therapy. Network impairments may contribute to the neuropsychological abnormalities in elderly HIV patients, who will soon account for around half of all HIV+ adults.

Key words: ApoE4; diffusion tensor imaging (DTI); fractional anisotropy (FA); geriatrics; high angular resolution diffusion imaging; imaging genetics; structural brain networks

Introduction

Infection with the human immunodeficiency virus (HIV) is a growing clinical complication in geriatric medicine. Approximately one-quarter of all HIV+ patients in the United States were over age 50 in 2005, a sharp increase from 17% in 2001 (CDC, 2007), with further increases expected. Since combination antiretroviral therapy (cART) became widely available, many sufferers of this viral epidemic are now living longer and more productive lives. Even so, the virus crosses the blood–brain barrier soon after infection (Gonzalez-Scarano and Martin-Garcia, 2005), enabling brain aberrations before patients show any signs or symptoms of disease (Valcour et al., 2012). In the course of infection, neuropsychological (NP) and cognitive deficits are noted in around half of all HIV+ adults (Heaton et al., 2010), in particular those with additional co-morbidities. Despite advances in treatment, postmortem studies show continued brain parenchymal infiltration of inflammatory cells (Langford et al., 2003). In older individuals, there is a concern that HIV may interact with the normal aging process, as cognitive impairment is over twice as common in older HIV+ people as in younger people who have been ill for the same amount of time (Valcour et al., 2004).

Brain mapping studies show thinner cortical gray matter in HIV+ patients (Thompson et al., 2005), and heavily affected white matter regions (Jernigan et al., 2011). The myelinated fibers that comprise the brain's white matter conduct signals between these cortical regions as well as subcortical regions. The relative levels of myelination and the degree of axonal packing can affect the rate and integrity of regional communication. *In vivo* diffusion-weighted magnetic resonance imaging (MRI) scanning can help capture these changes by mapping the estimated diffusion profile of water inside myelinated fibers. Disruptions in white matter integrity are seen in HIV+ patients with diffusion tensor imaging (DTI), and these changes are

[1]Imaging Genetics Center, Laboratory of Neuro Imaging, Department of Neurology, UCLA School of Medicine, Los Angeles, California.
[2]Medical Imaging Informatics Group, Department of Radiology, UCLA School of Medicine, Los Angeles, California.
[3]Department of Neurology, Memory and Aging Center, UCSF, San Francisco, California.
[4]Division of Geriatric Medicine, UCSF, San Francisco, California.
*Denotes equally contributing authors.

associated with cognitive decline (Tate et al., 2010) beyond that which is expected during normal aging (Chang et al., 2008). However, the way cortical regions in the brain are connected and the relative degrees to which they relay information to each other, or the brain's structural network, has yet to be studied in HIV populations.

To understand patterns of network breakdown and factors that affect it, we imaged 55 HIV+ and 30 age- and sex-matched HIV-seronegative individuals all aged 60–80. Through the use of multimodal brain scanning, including high-resolution anatomical images—to automatically extract functionally specialized cortical regions to define the network—and high angular resolution diffusion images (HARDI)—to trace the neural pathways of myelinated white matter tracts throughout the brain, we were able to map structural cortical connectivity disruptions associated with elderly carriers of the HIV virus. In our group of HIV+ patients, we expected to see altered brain connectivity in the frontal and motor systems that are typically impaired functionally and structurally. Moreover, treatment complications, as well as genetic risk factors for neurodegeneration, can precipitate neurological and cognitive decline. Carriers of the apolipoprotein E4 allele (ApoE4) are at a threefold increased risk for dementia, particularly Alzheimer's Disease (AD), and as a group, they show identifiable brain deficits before the onset of clinical symptoms (Reiman et al., 1996). In carriers of this risk gene, we hypothesized that neural networks would be even further disrupted, depending on the duration of infection.

Materials and Methods

Subject demographics

MRI, DTI, and clinical data were collected from HIV-infected participants enrolling in a larger longitudinal study of HIV, aging, and cognition at the Memory and Aging Center, University of California in San Francisco (UCSF). All participants were ambulatory and responded to advertisements for an HIV cognitive study or were referred by clinicians. Individuals with learning disabilities, major psychiatric or neurological illness, current or past brain infection, major systemic illness, or head injury with cognitive sequelae were excluded. There were 54 men and 2 women cases in total. All subjects received routine medical care with access to cART. Although not a requirement of the study, all but three subjects were on cART at the time of cognitive assessment. Among HIV+ subjects, all but six had undetectable plasma HIV RNA (defined as <400 copies/mL).

Age- and sex-matched HIV-negative individuals were selected from existing healthy aging cohorts at the UCSF that had all undergone the same imaging protocols as the HIV+ subjects. Controls were selected and imaged from a healthy aging cohort from San Francisco. Controls and patients were matched for sex and age as far as possible resulting in an approximate two subject-to-one control matching overall. The study was approved by the Institutional Review Boards of the UCSF and the University of California at Los Angeles School of Medicine. All participants signed informed written consent.

The NP test battery was completed by all patients to assess multiple cognitive domains, including memory, executive function, psychomotor speed, visuospatial skill, manual dexterity, and attention using the following tests: California Verbal Learning Test-II (16 item) trial 5, immediate and delayed recall trials, Story recall immediate and delayed recall trials, Benson Figure Copy and delayed recall, an internal modified Trails (set shifting) test, Trails A and B tests, Stroop color naming and interference trials, phonemic fluency with D-words, digits forward and backward, Digit Symbol Modalities test, Visual Object and Space Perception Battery, Grooved pegboard test-dominant and nondominant hands, and finger-tapping speed-dominant and nondominant hands. Individual standardized z-scores were calculated in a customary fashion using published normative data. For the Grooved Pegboard tests, internal normative data ($n=38$) were used. A summary NP z-score was calculated as the arithmetic mean of all individual z-scores.

Blood CD4+ lymphocyte counts and plasma HIV RNA levels were measured at a clinical lab for subjects without these measures within 3 months of their visit. As blood was collected for HIV+ patients only, a further investigation into their genetically determined dementia risk was conducted, but the controls were not genotyped. ApoE was genotyped real-time polymerase chain reaction (PCR) on an Applied Biosystems 7900HT Real Time PCR machine using TaqMan SNP Genotyping Assay for rs429358 and rs7412 with identification numbers C___3084793_20 and C____ 904973_10, respectively (Applied Biosystems, Foster City, CA). The protocol was followed as outlined in the manufacturer's instructions, and every assay was performed in duplicate. In addition to a standard curve amplification protocol, an allelic discrimination step was added to facilitate the contrast between the two alleles and their respective reporter dyes. SDS version 2.3 software was used to analyze the single-nucleotide polymorphism genotyping data. Nine out of 55 patients (16.4%) were carriers of the ApoE4 rs4420638 allele. This is in line with the 0.163 G-minor allele frequency reported from the 1000 Genomes Project for rs4420638 (http://ncbi.nlm.nih.gov/projects/SNP/snp_ref.cgi?rs=4420638). A report on 1186 elderly subjects (of average age 72) also found that 21.3% of individuals were carriers (of one or two copies) of the risk allele (Crivello et al., 2010).

MRI data acquisition

All subjects underwent whole-brain MRI on a Siemens 3 Tesla TIM Trio scanner with a 12-channel head coil. T1-weighted MP-RAGE sequences (240×256 matrix; field of view (FOV) = 256 mm; 160 slices; voxel size = $1.0\times1.0\times1.0$ mm^3; time to inversion = 900 msec; repetition time (TR) = 2300 msec; echo time (TE) = 2.98 msec; flip angle = 9°) and diffusion-weighted images (DWI) (100×100 matrix; FOV = 220 mm; 55 slices; voxel size = $2.2\times2.2\times2.2$ mm^3; TR = 8000 msec; TE = 109 msec) were collected; 65 images were acquired, one b_0 T2-weighted image with no diffusion sensitization and 64 DWI ($b=2000$ sec/mm^2). All T1-weighted MR and DWI images were quality checked visually to ensure that scans with excessive motion and/or artifacts were not included in the study. One male subject and one control were removed from the analysis as a result of image quality control, leaving a total of 53 men and 2 women cases.

DWI preprocessing, cortical surface extraction, and registrations

For each subject, all raw DWI volumes were aligned to the b_0 image (DTI volume with no diffusion sensitization) using

FSL (www.fmrib.ox.ac.uk/fsl) to correct for head motion and eddy current distortions. All extracerebral tissue was subsequently removed from the T1-weighted scans using ROBEX (Iglesias et al., 2011) and from the DWI images using the Brain Extraction Tool from FSL. To ensure alignment in space, each T1-weighted image was linearly aligned to a standard template—the Colin27 (Holmes et al., 1998)—using FSLs FLIRT with 9 degrees of freedom to account for translations, rotations, and scaling in 3D. To correct for echo planar imaging (EPI)-induced susceptibility artifacts, which can cause distortions at tissue–fluid interfaces, skull-stripped b_0 images were linearly aligned and then elastically registered to their respective T1-weighted structural scans using an inverse consistent registration algorithm with a mutual information cost function (Leow et al., 2007). The resulting 3D deformation fields were subsequently applied to the remaining 64 DWI volumes before tensor calculations.

A single diffusion tensor was modeled at each voxel in the brain from the corrected DWI scans using FSL. Fractional anisotropy maps were obtained from the resulting diffusion tensor eigenvalues (λ_1, λ_2, and λ_3) (Basser and Pierpaoli, 1996).

We automatically extracted 34 cortical labels per hemisphere (Table 1) from T1-weighted structural MRI scans using FreeSurfer (http://surfer.nmr.mgh.harvard.edu/). Region 4 was not delineated in the 5.0 version of FreeSurfer, and therefore all connections in those regions were not considered. T1-weighted images and cortical labels were down-sampled using nearest neighbor interpolation (to avoid intermixing of labels) to the space of the linearly registered DWIs. To ensure that tracts would intersect cortical labeled boundaries, labels were dilated with an isotropic box kernel of $5\times5\times5$ voxels.

Fiber tractography and matrix creation

At each HARDI voxel, orientation distribution functions (ODFs) were computed using the normalized and dimensionless ODF estimator, derived for Q-ball imaging (Aganj et al., 2010). Global tractography was performed on the linearly aligned sets of ODF volumes by probabilistically seeding voxels with a prior probability based on the fractional anisotrophy (FA) value. Curves through a seed point receive a score estimating the probability of the existence, computed from the ODFs. We used a voting process provided by the Hough transform to determine the best-fitting curves through each point. Further details of the method may be found in Aganj et al. (2011).

Elastic deformations obtained from the EPI distortion correction, mapping the average b_0 image to the T1-weighted image, were then applied to the tracts' 3D coordinates. Each subject's dataset contained $\sim$20,000 useable fibers (3D curves), nonduplicated tracts consisting of more than 5 traced points. Fibers were drawn with a 0.2-voxel resolution, so 5 points are equivalent to 1 voxel or 2 mm in length; shorter fibers were removed. We additionally removed any erroneous fibers traced on the edge of the brain due to high-intensity noise.

For each subject, two full 68×68 connectivity matrices were created: one describing the relative fiber density of connections, and another examining the average FA along the tracts of the connections. In the case of the fiber density matrices, each element described the estimated proportion of the total number of fibers, in that subject, connecting each of the labels in one region to those in the other. Fibers were counted in the matrix if the fiber crossed a region or intersected two regions of interest (ROIs). The mean FA along the tract was calculated, and the values were stored in a new matrix whose elements reflect the mean FA along each connection.

There are several reasonable ways to construct maps of anatomical connectivity—it is possible to define the edge weights in various ways (Duarte-Carvajalino et al., 2012), and several different parcellation schemes have been advocated and used. Here we chose to study a set of nodes as defined by the cortical regions in the standard and widely used Desikan–Killiany atlas (Desikan et al., 2006). To define edge weights for the connections between these regions, we chose to use the proportion of fibers traveling between the regions, as a fraction of the total number of fibers detected in the brain. This definition leads to a symmetric matrix, and it also can be used to highlight the aggregate fiber density emanating from any particular ROI to all other regions being considered.

Additionally, to confirm that the connections we found to be significantly different between patients and controls in our

Table 1. List of the Cortical Labels Extracted from FreeSurfer

1	Banks of the superior temporal sulcus	19	*Pars orbitalis*
2	Caudal anterior cingulate	20	*Pars triangularis*
3	Caudal middle frontal	21	Pericalcarine
4	Corpus callosum	22	Postcentral
5	Cuneus	23	Posterior cingulate
6	Entorhinal	24	Pre-central
7	Fusiform	25	Precuneus
8	Inferior parietal	26	Rostral anterior cingulate
9	Inferior temporal	27	Rostral middle frontal
10	Isthmus of the cingulate	28	Superior frontal
11	Lateral occipital	29	Superior parietal
12	Lateral orbitofrontal	30	Superior temporal
13	Lingual	31	Supra-marginal
14	Medial orbitofrontal	32	Frontal pole
15	Middle temporal	33	Temporal pole
16	Parahippocampal	34	Transverse temporal
17	Paracentral	35	Insula
18	*Pars opercularis*		

analysis were due to loss of connecting fibers rather than differences in fibers originating from any particular ROI (which can be influenced by ROI size differences itself between groups), a second normalization was performed such that off-diagonal matrix elements were normalized by the number of fibers that cross each of the individual connections, to control for the relative number of fibers in ROIs.

Therefore, if $A(i,j)$ is the original fiber count matrix, for the newly normalized matrix B, element (i,j),

$$B(i,j) = \frac{A(i,j)}{A(i,i) + A(j,j) - A(i,j)}$$

that is, diagonal elements will be equal to 1, and off-diagonal elements will be proportional to the total number of fibers in each of the intersecting ROIs, rather than the total number of fibers overall. This normalization will overcome the possibility that a region with larger fibers would influence the connection. Note that this normalization will allow us to only determine independent fiber effects within off-diagonal elements.

Calculation of network properties

At the nodal level, where each of the 68 cortical regions is considered a node, we calculated the relative weighted (by the density of fiber connections) number of regions each ROI was directly connected to, that is, the strength of the node, as well as local efficiency, using functions from the brain connectivity toolbox (http://brain-connectivity-toolbox.net/). Local efficiency declines with aging and dementia, and is thought to measure the information processing capability (Pievani et al., 2011).

Statistical analysis

In anatomical connectivity analysis, different connections vary in their ability to achieve sufficient statistical power to detect differences in the population. This can be for a variety of reasons, including the size of the regions of interest being connected and the physical length of the connections between the regions. For example, smaller regions may not have a stable or sufficient proportion of streamline fibers running through them, and the resulting variance may make it more difficult to pick up systematic statistical effects on those regions and connections. Here, we aim to eliminate unnecessary testing on extremely low-powered connections by ensuring that at least 50% of all subjects included in a statistical test had fibers connecting the test region. Statistical analysis was performed on every matrix element for which at least 50% of the subjects had a connection. To control for the multiple comparisons inherent in this work, we used the standard false discovery rate (FDR; Benjamini and Hochberg, 1995) procedure, setting the false-positive rate at $q = 0.05$. As all matrices in this analysis were symmetric, FDR correction was performed on the diagonal and lower triangular portion of the resulting p-value matrix.

Linear regression was performed simultaneously adjusting for the linear effects of age and sex. The analyses were implemented in the R statistical package (version 2.9.2; http://r-project.org/) using the nlme library (Pinheiro and Bates, 2000).

We first considered a full multilinear model, including age, sex, ApoE4 status, duration of HIV infection, the interaction between age and ApoE4 status, and the interaction between HIV duration and ApoE4 status. We started from the full set of predictors and removed covariates that did not improve the fit from the model step-by-step. As standard covariates, age and sex were kept in the model. Log likelihoods of full-versus-partial models were assessed with a χ^2 test. A model was considered to better fit the data if the difference in χ^2 values between it and the more comprehensive model at the previous step was not significant. If two models contained the same number of parameters, the model with a smaller χ^2 value was considered the better one. Model selection ended when the best model was achieved, that is, when all possible more restricted models were not better than the current model.

To assess the effect of joint variables, a partial F-test method was used where the combined effects of the additional predictors (ApoE4 and ApoE4 by duration of HIV) were assessed by comparing the full model (age, sex, ApoE4, and ApoE4 by duration of HIV) to a partial model with that of just sex and age alone.

Results

Patient demographics are shown in Table 2. Fifty-five HIV+ patients, aged 60–80 years, were compared to 30 age-matched controls. Nine HIV patients were also carriers of the ApoE4 risk allele, of whom one was homozygous (i.e., carried two copies of ApoE4). The HIV+ ApoE4 carriers and noncarriers did not differ in age ($p = 0.43$). All patients and controls had at least a high school level of education, but controls had on average slightly higher educational levels. All but 6 HIV patients had undetectable viral loads.

Structural brain networks were computed from the brain MRI scans and diffusion images, for patients and controls. Networks were compared statistically to identify connections that differed in the HIV+ group versus controls. Deficits in

Table 2. Subject Demographics

	HIV−	*HIV+*	p-*Value*
Total N (women)	30 (4)	55 (2)	—
Age, years (SD)	65.3 (2.2)	64.0 (3.7)	0.08
Education, years (SD)	17.4 (2.1)	16.1 (2.2)	0.008
CD4+ T-cell count, nadir (SD)	—	206.6 (190.1)	—
Duration of infection, years (SD; $N = 53$)	—	20.1 (6.4)	—
ApoE4 carriers (non)	—	9 (46)	—

Fifty-five HIV+ patients aged 60–80 were compared to 30 age-matched controls.
SD, standard deviation; ApoE4, apolipoprotein E4 allele; HIV, human immunodeficiency virus.

the proportion of fibers were found for both the left and right superior frontal cortex in HIV+ patients compared to controls. Patients also showed altered patterns of connections between the right superior frontal cortex and the right precentral cortex, the right precentral cortex and the right posterior cingulate, the right posterior cingulate and the left superior frontal cortex, and the right inferior parietal cortex and the right isthmus of the cingulate (Fig. 1). Furthermore, the connection strength of each cortical region was also altered. The strength of each node in a network is defined as the number of other nodes it is connected to, in this case weighted by the fiber density of each connection. After correcting for multiple comparisons across all cortical regions, HIV+ subjects showed weaker connections to and from the left paracentral, the left and right posterior cingulate, the left and right superior frontal, and the right caudal anterior cingulate cortices, all regions where cortical atrophy is prevalent in HIV. As mentioned previously, several studies show white matter integrity differences between HIV patients and controls in large white matter tracts. While we report differences in the fiber densities of the connections shared by the majority of the cohort, we do not find FA differences along the HARDI cortical connection fibers. Note that this does not reflect whether there are white matter integrity differences in major tracts, but that the integrity along cortical connections was not significant, in this case. Our HARDI tractography was performed taking into account possible shortcomings of the single-tensor model, while FA is a measure based on the diffusion tensor. These complementary analyses offer an expanded explanation into the possible differences in the anatomical network, as fibers may be deteriorating, even in samples where FA-based measures of integrity do not yet differ significantly between patients and controls.

ApoE4 genotype in HIV+

We examined the effect of carrying at least one ApoE4 allele (testing carriers vs. noncarriers as two groups) on fiber integrity measured along fibers connecting cortical regions. Although there were relatively few carriers ($N=9$) compared to noncarriers ($N=46$), significant differences were found.

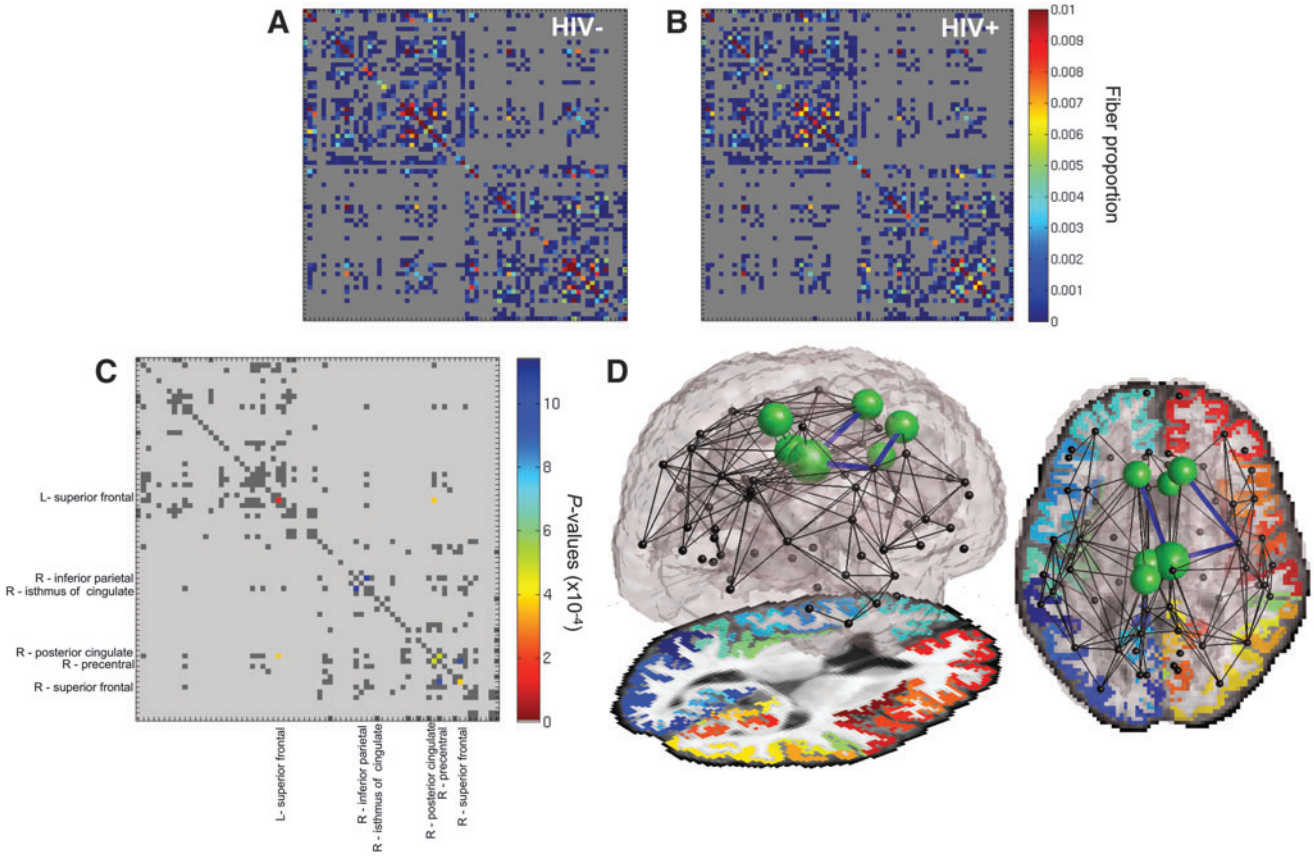

FIG. 1. The proportion of fibers connecting cortical regions is altered in the presence of human immunodeficiency virus (HIV). The average connectivity matrices for **(A)** 30 HIV− subjects and **(B)** for 55 HIV+ participants are shown; **(C)** controlling for effects of age and sex, HIV+ participants show lower fiber densities in the left and right superior frontal cortices, and in the connections between the right superior frontal cortex and the right precentral cortex, the right precentral cortex and right posterior cingulate, the right posterior cingulate and left superior frontal cortex, and the right inferior parietal and right isthmus of the cingulate. Tested connections (i.e., those present in >50% of individuals) are *dark gray*; **(D)** the significant intercortical connections are shown again (*blue lines*). Nonsignificant tested connections are in *black*. The connection strength (defined as the total fiber density of connections for each region) is significantly lower in the presence of the virus (*green spheres*) in the left paracentral, the left and right posterior cingulate, the left and right superior frontal, and the right caudal anterior cingulate. In the *top view*, the left hemisphere is shown on the left. Larger spheres indicate greater effect sizes (lower *p*-values).

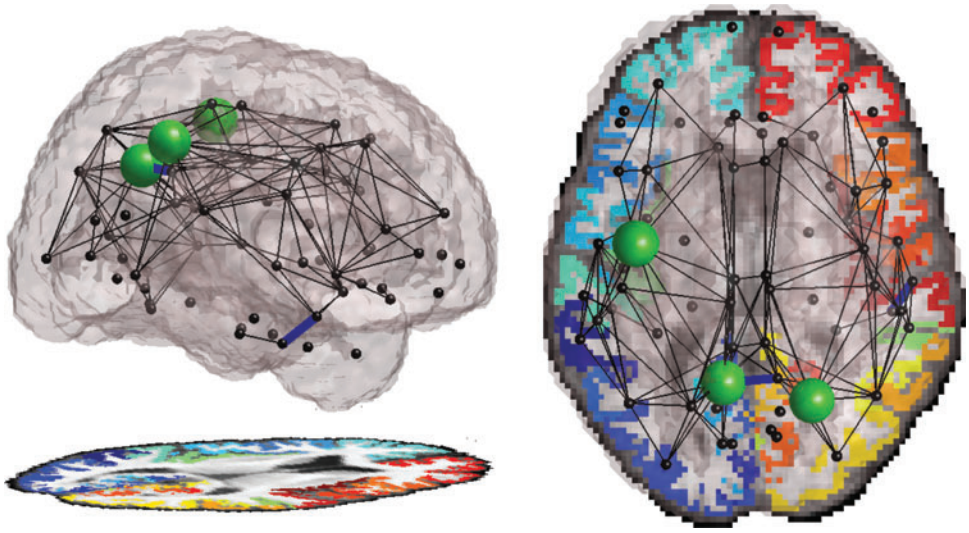

FIG. 2. HIV+ individuals who also carry a copy of the apolipoprotein E4 (ApoE4) Alzheimer's disease risk allele ($N=9$) have impaired cortical connections, compared to HIV+ people who do not carry the ApoE4 risk allele ($N=46$). The connection between the right inferior and medial temporal gyri, as well as the connection between the left and right precuneus, shows significantly reduced FA (shown as *blue lines* connecting those nodes). Also the local efficiency of the connections to and from the left precentral gyrus, left precuneus, and right superior parietal cortices are significantly reduced (*green spheres* are proportional in size to $-\log(p)$, the negative logarithm of the p-value of the association).

Carriers and noncarriers did not differ in mean age ($p=0.43$), CD4 nadir T-cell count ($p=0.41$), RNA viral load ($p=0.17$), or the summary NP z-score ($p=0.70$). The connection between the right inferior and medial temporal gyri, as well as the connection between the left and right precuneus, showed significantly lower FA (Fig. 2). The mean FA in the right inferior temporal lobe and the right precuneus was also significantly lower in the ApoE4 carriers. Additionally, we computed the local efficiency for each cortical region. The efficiency of the left precentral gyrus, left precuneus, and right superior parietal cortices was significantly impaired in the HIV+ group. We found no effect of the interaction of ApoE4 and age in our population.

ApoE4 and HIV infection duration

Self-report of the duration of infection was available for 53/55 subjects (all but two ApoE4 noncarriers). Duration alone had no statistical effect on the connectivity pattern, but the ApoE4 status interacted with the duration of HIV infection to significantly alter the connectivity pattern.

When analyzed jointly, the ApoE4 status and its interaction with duration of HIV infection together showed associations with the integrity in connections between the left supramarginal and precentral cortex, the left supramarginal cortex and left insula, and the right isthmus of the cingulate with the posterior cingulate. Additionally, the mean fiber integrity within the tracts of right superior temporal cortex and in the supramarginal cortex also showed an effect of ApoE4. The nodal efficiency of the left precentral gyrus, the left precuneus, left superior temporal cortex, and the right superior parietal, and right supramarginal cortices. These regions are shown in Figure 3A.

Individually, as seen in Figure 3B, the interaction term (when controlling for the main effect of ApoE4) additionally showed reduced fiber integrity for the connection between the left supramarginal cortex and the precentral cortex. The FA and nodal efficiency are also reduced in the right supramarginal cortex.

For tests performed within the HIV+ population, we find no differences in the density of fibers within the group or the strength of the connections, yet the integrity of the connections as indexed by FA is compromised along with the corresponding efficiency.

Discussion

In this study, we use advanced imaging techniques to map the cortical network in older HIV+ patients and age-matched controls. We define this structural network as the density and integrity of white matter connections between cortical regions. As compared to the aged-matched HIV– population, we found a broad disruption in brain connectivity in older individuals infected with the virus. Fiber concentrations were compromised mainly in frontal and motor regions. As ApoE4 is the greatest genetic risk factor for dementia, we further compared HIV+ individuals with this genotype to those noncarriers. We found that those who also carry the ApoE4 risk allele showed additional network deficits in temporal and parietal regions. Upon further investigation, we found that the ApoE4 genotype interacted with of the duration of HIV infection, with greater network deficits in ApoE4 carriers with prolonged viral infection, suggesting continual interaction of the virus and the gene.

Histological studies find lower neuronal concentrations in cortices of individuals who died with HIV infection compared to seronegative individuals (Everall et al., 1991). While a recent study of functional connectivity in HIV+ individuals suggested altered occipital lobe connectivity (Wang et al., 2011), in our older cohort, cortical connectivity was

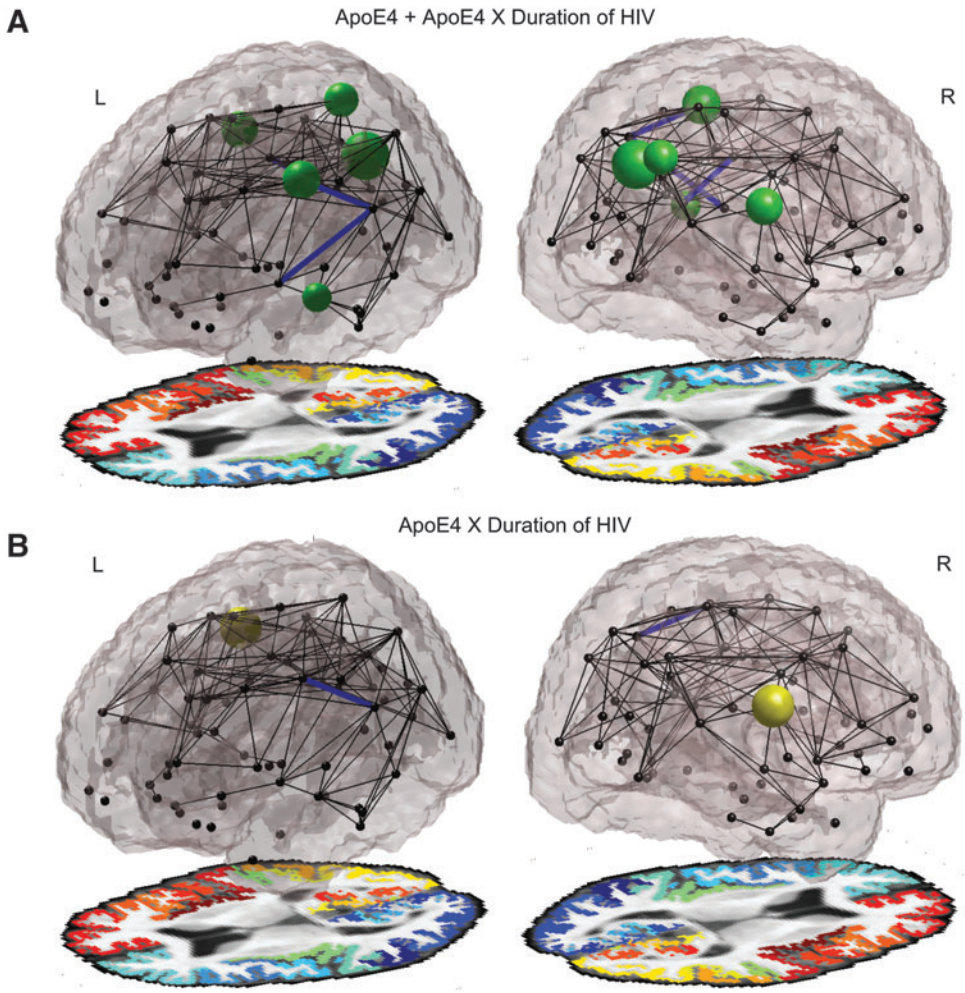

FIG. 3. **(A)** ApoE4 status and its interaction with HIV duration together show associations with the integrity in connections (*blue lines*) between the left supramarginal and precentral cortex, the left supramarginal cortex and left insula, and the right isthmus of the cingulate with the posterior cingulate. The mean fiber integrity of the tracts of the right superior temporal cortex and supramarginal cortex also show ApoE4 effects. The nodal efficiency (*green spheres*) of the left precentral gyrus, the left precuneus, left superior temporal cortex, and the right superior parietal and right supramarginal cortices, additionally show a reduction when jointly evaluating ApoE4 and the interaction between ApoE4 and the self-reported duration of infection. **(B)** Individually, the interaction term (when controlling for the effect of ApoE4) showed reduced fiber integrity in the connection between the left supramarginal cortex and the precentral cortex. The FA and efficiency are also reduced in the right supramarginal cortex. Larger spheres are associated with greater effect sizes (lower *p*-values). The left hemisphere is colored blue-green, and the right hemisphere is colored red-yellow.

altered in more frontal-parietal regions, consistent with the known profile of cortical atrophy in HIV (Fig. 1). This finding is congruent with cortical thinning patterns (Thompson et al., 2005) and reduced cortical volumes (Cohen et al., 2010) in younger HIV+ cohorts. In HIV, the frontal lobes are implicated as a major region of altered white matter structure (Pomara et al., 2001), biochemical composition (Lopez-Villegas et al., 1997), and as a contributor to several cognitive impairments, such as impaired concentration and motor control. Premotor cortex and superior frontal cortices showed impaired connectivity here. In our connectivity analysis here, we specifically find that the superior frontal cortices themselves show deficits in the number of fibers that cross the regions (results lying on the matrix diagonal) in addition to fibers connecting to other brain regions (off-diagonal elements). Results on the diagonal may suggest that the specific region may be particularly harmed in the disease, confirming results from prior studies; yet, through connectivity analysis, we can further map the connecting regions of the brain most altered by the marked anatomical decline in these regions. Deficits in the ability of these regions to relay signals and communicate may contribute to the behavioral and cognitive symptoms observed in this population.

The corpus callosum, the primary white matter structure connecting the two brain hemispheres, shows thinning (Thompson et al., 2006) and altered integrity (Wu et al., 2006) in the presence of HIV infection. In our study, interhemispheric connections were impaired between the left and right superior frontal cortices, and altered white matter structure in the corpus callosum may underlie some of the frontal deficits and connectivity disruptions prevalent in the HIV+ population.

As well as evaluating element-wise cortical connections, hierarchical network measures can examine brain networks on a more global scale to reveal differences and variations within a population (Duarte-Carvajalino et al., 2012). Nodal efficiency in particular—which may measure information processing capability (Pievani et al., 2011)—declines with aging and dementia, especially in the frontal and temporal regions (Wen et al., 2011). Structural (Lo et al., 2010) analyses also report poorer local efficiency in elderly individuals with AD.

Several genes are expressed differently in the HIV-seropositive cortex (Masliah et al., 2004). Patients with HIV-associated dementia differentially express some proteins in metabolic pathways critical for the pathogenesis of AD (Zhou et al., 2010). This altered profile of gene expression may increase dementia risk in HIV+ individuals, but it is largely unknown which brain networks are disrupted, and whether network alterations differ from those typical of normal aging. As studies of the connectome are just becoming feasible, with advances in brain scans that can reconstruct neural pathways and their connections, we were able to map the connections in elder HIV+ individuals to determine how the viral interaction with genetic risk factors for dementia combine to alter brain wiring. Even so, much debate surrounds the validity of fiber counts as a measure of anatomical connectivity. Fiber counts derived from diffusion images are not in themselves a measure of connection strength, and they offer an indirect, surrogate measure of true anatomical fiber connectivity—which cannot be measured directly when people are alive (and not in a large post-mortem population, for that matter). This measure of fiber distribution is found to highlight meaningful differences in this study. Limitations of diffusion-based assessments of connectivity and other methods are discussed further in (Jbabdi and Johansen-Berg, 2011).

In this study, we examined the efficiency of each cortical region as a function of a primary dementia risk factor, the carriers of the ApoE4 allele, within the HIV+ population and found significant reductions in efficiency in carriers, despite the fact that no overall NP differences were observed between genotype groups. Additionally, we found that the altered brain connectivity network further correlated with the interaction between the duration of infection and the genotype, suggesting that lengthened viral and genetic interactions continually lead to the degrading of connections within the brain. However, our study is limited in the number of subjects where a genotype by disease duration effect was found, and these results should be verified in further studies.

Age-associated brain changes may contribute to cognitive decline as HIV+ patients get older. Some pathological changes in the brains of HIV+ people are caused by indirect mechanisms, not by the virus directly (Gonzalez-Scarano and Martin-Garcia 2005). In a recent independent study of structural connectivity in carriers of the ApoE4 allele (Brown et al., 2011), disrupted cortical connections were found in regions overlapping with those found here. In our study, the mean FA in fibers along the right inferior temporal cortex and those along the fibers of the right precuneus were significantly lower in carriers than noncarriers. Despite differences in methods, Brown et al. (2011) found that regions, including the precuneus and inferior temporal gyrus, exhibited significant age-by-ApoE4 interactions when examining clustering coefficient across the network. We did not find an age-by-ApoE4 interaction in our study, possibly due to the narrower age range. However, the repeated associations of these same cortical regions to this risk gene may confirm the role that the precuneus and temporal regions play in the genetic risk for dementia. Lower fiber integrity in these regions may also underlie some of the deficits found in functional connectivity studies for ApoE4 carriers (Sheline et al., 2010).

The supramarginal gyrus in the parietal lobe is repeatedly implicated in cases of dementia. Neurofibrillary tangles and neuronal loss in the region are correlated with intellectual status in elderly women (Grignon et al., 1998). The volume of the supramarginal gyrus declines in ApoE4 carriers as they convert from mild cognitive impairment to AD (Spampinato et al., 2011). In a diffusion-based study, the regions underlying the gyrus showed suggestive negative associations between FA and age in HIV patients (Gongvatana et al., 2011). Brown et al. (2011) also found a significant genetic effect in the supramarginal gyrus. Here, the duration of HIV interacted with the ApoE4 status to influence the integrity of the supramarginal gyrus, even when controlling for ApoE4 status alone. These additional disruptions could reflect a continual genetic interaction with the virus, especially in brain regions highly susceptible to amyloid accumulation and neurofibrillary tangles. While ApoE4 has been associated with faster disease progression in HIV+ individuals (Burt et al., 2008), its effects in elderly cohorts may not be identical to those found in younger people, in part because the gene impacts survival, making it vital to confirm these associations in younger cohorts.

Conclusion

In summary, aged HIV+ subjects show altered brain connectivity and integrity, differences that are further exacerbated in carriers of the ApoE4 genotype. Examining changes in the structural composition of the aging HIV+ brain may enable greater insight into the neuronal pathways targeted by infection and further complicated by genetic susceptibility. This work isolates neuropathological alterations in those living with HIV despite today's cART availability and highlights the additional network disruptions seen in HIV+ individuals aging alongside those without the virus. These network alterations provide an anatomical basis for the additional NP abnormalities seen in elderly HIV patients, a crucial insight, as this elderly group may soon comprise nearly 50% of all community-dwelling HIV+ adults.

Acknowledgments

This study was supported by the following grants: K23AG032872 (to V.G.V.), P50 AG023501 (ADRC, PI: Bruce Miller); P30-AI027763 (UCSF CFAR), UL1 RR024131 (UCSF GCRC), the Larry L. Hillblom Foundation and the AIDS Research Institute at UCSF. N.J., T.M.N. O.K., and P.M.T. were supported in part by the National Institute for Biological Imaging and Bioengineering (R01 EB008432, R01 EB007813, and P41 RR013642 to P.M.T.). N.J. was supported in part by the NIH NLM Grant T15 LM07356.

Author Disclosure Statement

No competing financial interests exist.

References

Aganj I, Lenglet C, Jahanshad N, Yacoub E, Harel N, Thompson PM, Sapiro G. 2011. A Hough transform global probabilistic approach to multiple-subject diffusion MRI tractography. Med Image Anal 15:414–425.

Aganj I, Lenglet C, Sapiro G, Yacoub E, Uğurbil K, Harel N. 2010. Reconstruction of the orientation distribution function in single- and multiple-shell q-ball imaging within constant solid angle. Magn Reson Med 64:554–566.

Basser PJ, Pierpaoli C. 1996. Microstructural and physiological features of tissues elucidated by quantitative-diffusion-tensor MRI. J Magn Reson B 111:209–219.

Benjamini Y, Hochberg Y. 1995. Controlling the false discovery rate - a practical and powerful approach to multiple testing. J Roy Stat Soc B Met 57:289–300.

Brown JA, Terashima KH, Burggren AC, Ercoli LM, Miller KJ, Small GW, Bookheimer SY. 2011. Brain network local interconnectivity loss in aging APOE-4 allele carriers. Proc Natl Acad Sci U S A 108:20760–20765.

Burt TD, Agan BK, Marconi VC, He W, Kulkarni H, Mold JE, Cavrois M, Huang Y, Mahley RW, Dolan MJ, McCune JM, Ahuja SK. 2008. Apolipoprotein (apo) E4 enhances HIV-1 cell entry *in vitro*, and the APOE epsilon4/epsilon4 genotype accelerates HIV disease progression. Proc Natl Acad Sci U S A 105:8718–8723.

CDC. 2007. HIV/AIDS Surveillance Report, 2005. In: *US Department of Health and Human Services*, vol. 17. Atlanta: CDC, pp. 1–54.

Chang L, Wong V, Nakama H, Watters M, Ramones D, Miller EN, Cloak C, Ernst T. 2008. Greater than age-related changes in brain diffusion of HIV patients after 1 year. J Neuroimmune Pharmacol 3:265–274.

Cohen RA, Harezlak J, Schifitto G, Hana G, Clark U, Gongvatana A, Paul R, Taylor M, Thompson P, Alger J, Brown M, Zhong J, Campbell T, Singer E, Daar E, McMahon D, Tso Y, Yiannoutsos CT, Navia B. 2010. Effects of nadir CD4 count and duration of human immunodeficiency virus infection on brain volumes in the highly active antiretroviral therapy era. J Neurovirol 16:25–32.

Crivello F, Lemaitre H, Dufouil C, Grassiot B, Delcroix N, Tzourio-Mazoyer N, Tzourio C, Mazoyer B. 2010. Effects of ApoE-epsilon4 allele load and age on the rates of grey matter and hippocampal volumes loss in a longitudinal cohort of 1186 healthy elderly persons. Neuroimage 53:1064–1069.

Desikan RS, Segonne F, Fischl B, Quinn BT, Dickerson BC, Blacker D, Buckner RL, Dale AM, Maguire RP, Hyman BT, Albert MS, Killiany RJ. 2006. An automated labeling system for subdividing the human cerebral cortex on MRI scans into gyral based regions of interest. Neuroimage 31:968–980.

Duarte-Carvajalino JM, Jahanshad N, Lenglet C, McMahon KL, de Zubicaray GI, Martin NG, Wright MJ, Thompson PM, Sapiro G. 2012. Hierarchical topological network analysis of anatomical human brain connectivity and differences related to sex and kinship. Neuroimage 59:3784–3804.

Everall IP, Luthert PJ, Lantos PL. 1991. Neuronal loss in the frontal cortex in HIV infection. Lancet 337:1119–1121.

Gongvatana A, Cohen RA, Correia S, Devlin KN, Miles J, Kang H, Ombao H, Navia B, Laidlaw DH, Tashima KT. 2011. Clinical contributors to cerebral white matter integrity in HIV-infected individuals. J Neurovirol 17:477–486.

Gonzalez-Scarano F, Martin-Garcia J. 2005. The neuropathogenesis of AIDS. Nat Rev Immunol 5:69–81.

Grignon Y, Duyckaerts C, Bennecib M, Hauw JJ. 1998. Cytoarchitectonic alterations in the supramarginal gyrus of late onset Alzheimer's disease. Acta Neuropathol 95:395–406.

Heaton RK, Clifford DB, Franklin DR, Jr., Woods SP, Ake C, Vaida F, Ellis RJ, Letendre SL, Marcotte TD, Atkinson JH, Rivera-Mindt M, Vigil OR, Taylor MJ, Collier AC, Marra CM, Gelman BB, McArthur JC, Morgello S, Simpson DM, McCutchan JA, Abramson I, Gamst A, Fennema-Notestine C, Jernigan TL, Wong J, Grant I. 2010. HIV-associated neurocognitive disorders persist in the era of potent antiretroviral therapy: CHARTER Study. Neurology 75:2087–2096.

Holmes CJ, Hoge R, Collins L, Woods R, Toga AW, Evans AC. 1998. Enhancement of MR images using registration for signal averaging. J Comput Assist Tomogr 22:324–333.

Iglesias JE, Liu CY, Thompson PM, Tu Z. 2011. Robust brain extraction across datasets and comparison with publicly available methods. IEEE Trans Med Imaging 30:1617–1634.

Jbabdi S, Johansen-Berg H. 2011. Tractography: where do we go from here? Brain Connect 1:169–183.

Jernigan TL, Archibald SL, Fennema-Notestine C, Taylor MJ, Theilmann RJ, Julaton MD, Notestine RJ, Wolfson T, Letendre SL, Ellis RJ, Heaton RK, Gamst AC, Franklin DR, Jr., Clifford DB, Collier AC, Gelman BB, Marra C, McArthur JC, McCutchan JA, Morgello S, Simpson DM, Grant I. 2011. Clinical factors related to brain structure in HIV: the CHARTER study. J Neurovirol 17:248–257.

Langford TD, Letendre SL, Larrea GJ, Masliah E. 2003. Changing patterns in the neuropathogenesis of HIV during the HAART era. Brain Pathol 13:195–210.

Leow AD, Yanovsky I, Chiang MC, Lee AD, Klunder AD, Lu A, Becker JT, Davis SW, Toga AW, Thompson PM. 2007. Statistical properties of Jacobian maps and the realization of unbiased large-deformation nonlinear image registration. IEEE Trans Med Imaging 26:822–832.

Lo CY, Wang PN, Chou KH, Wang J, He Y, Lin CP. 2010. Diffusion tensor tractography reveals abnormal topological organization in structural cortical networks in Alzheimer's disease. J Neurosci 30:16876–16885.

Lopez-Villegas D, Lenkinski RE, Frank I. 1997. Biochemical changes in the frontal lobe of HIV-infected individuals detected by magnetic resonance spectroscopy. Proc Natl Acad Sci U S A 94:9854–9859.

Masliah E, Roberts ES, Langford D, Everall I, Crews L, Adame A, Rockenstein E, Fox HS. 2004. Patterns of gene dysregulation in the frontal cortex of patients with HIV encephalitis. J Neuroimmunol 157:163–175.

Pievani M, de Haan W, Wu T, Seeley WW, Frisoni GB. 2011. Functional network disruption in the degenerative dementias. Lancet Neurol 10:829–843.

Pinheiro JC, Bates DM. 2000. *Mixed-Effects Models in S and S-PLUS*. New York: Springer.

Pomara N, Crandall DT, Choi SJ, Johnson G, Lim KO. 2001. White matter abnormalities in HIV-1 infection: a diffusion tensor imaging study. Psychiatry Res 106:15–24.

Reiman EM, Caselli RJ, Yun LS, Chen K, Bandy D, Minoshima S, Thibodeau SN, Osborne D. 1996. Preclinical evidence of Alzheimer's disease in persons homozygous for the epsilon 4 allele for apolipoprotein E. N Engl J Med 334:752–758.

Sheline YI, Morris JC, Snyder AZ, Price JL, Yan Z, D'Angelo G, Liu C, Dixit S, Benzinger T, Fagan A, Goate A, Mintun MA. 2010. APOE4 allele disrupts resting state fMRI connectivity in the absence of amyloid plaques or decreased CSF Abeta42. J Neurosci 30:17035–17040.

Spampinato MV, Rumboldt Z, Hosker RJ, Mintzer JE. 2011. Apolipoprotein E and gray matter volume loss in patients with mild cognitive impairment and Alzheimer disease. Radiology 258:843–852.

Tate DF, Conley J, Paul RH, Coop K, Zhang S, Zhou W, Laidlaw DH, Taylor LE, Flanigan T, Navia B, Cohen R, Tashima K. 2010. Quantitative diffusion tensor imaging tractography metrics are associated with cognitive performance among HIV-infected patients. Brain Imaging Behav 4:68–79.

Thompson PM, Dutton RA, Hayashi KM, Lu A, Lee SE, Lee JY, Lopez OL, Aizenstein HJ, Toga AW, Becker JT. 2006. 3D mapping of ventricular and corpus callosum abnormalities in HIV/AIDS. Neuroimage 31:12–23.

Thompson PM, Dutton RA, Hayashi KM, Toga AW, Lopez OL, Aizenstein HJ, Becker JT. 2005. Thinning of the cerebral cortex visualized in HIV/AIDS reflects CD4+ T lymphocyte decline. Proc Natl Acad Sci U S A 102:15647–15652.

Valcour V, Chalermchai T, Sailasuta N, Marovich M, Lerdlum S, Suttichom D, Suwanwela NC, Jagodzinski L, Michael N, Spudich S, Souza FvGMd, Kim J, Ananworanich J, the RV254/SEARCH 010 Study Group. 2012. CNS viral invasion and inflammation during acute HIV. J Infect Dis 206:275–282.

Valcour V, Shikuma C, Shiramizu B, Watters M, Poff P, Selnes O, Holck P, Grove J, Sacktor N. 2004. Higher frequency of dementia in older HIV-1 individuals: the Hawaii aging with HIV-1 cohort. Neurology 63:822–827.

Wang X, Foryt P, Ochs R, Chung J-H, Wu Y, Parrish T, Ragin AB. 2011. Abnormalities in resting-state functional connectivity in early human immunodeficiency virus infection. Brain Connectivity 1:207–217.

Wen W, Zhu W, He Y, Kochan NA, Reppermund S, Slavin MJ, Brodaty H, Crawford J, Xia A, Sachdev P. 2011. Discrete neuroanatomical networks are associated with specific cognitive abilities in old age. J Neurosci 31:1204–1212.

Wu Y, Storey P, Cohen BA, Epstein LG, Edelman RR, Ragin AB. 2006. Diffusion alterations in corpus callosum of patients with HIV. AJNR Am J Neuroradiol 27:656–660.

Zhou L, Diefenbach E, Crossett B, Tran SL, Ng T, Rizos H, Rua R, Wang B, Kapur A, Gandhi K, Brew BJ, Saksena NK. 2010. First evidence of overlaps between HIV-Associated Dementia (HAD) and non-viral neurodegenerative diseases: proteomic analysis of the frontal cortex from HIV+ patients with and without dementia. Mol Neurodegener 5:27.

Address correspondence to:
Paul M. Thompson
Laboratory of Neuro Imaging
Department of Neurology
Imaging Genetics Center
UCLA School of Medicine
Neuroscience Research Building 225E
635 Charles Young Drive
Los Angeles, CA 90095-1769

E-mail: thompson@loni.ucla.edu